Effect of surface morphology on Tungsten sputtering yields

Lopez Cazalilla, Alvaro

2022

Lopez Cazalilla , A , Jussila , J , Nordlund , K & Granberg , F 2022 , ' Effect of surface morphology on Tungsten sputtering yields ' , Computational Materials Science , vol. 216 , no. 111876 . https://doi.org/10.1016/j.commatsci.2022.111876

http://hdl.handle.net/10138/350763
https://doi.org/10.1016/j.commatsci.2022.111876

Computational Materials Science 216 (2023) 111876

Contents lists available at ScienceDirect

Computational Materials Science

journal homepage: www.elsevier.com/locate/commatsci

Full length article

Effect of surface morphology on Tungsten sputtering yields

Alvaro Lopez-Cazalilla *, Joonas Jussila, Kai Nordlund, Fredric Granberg

Department of Physics, University of Helsinki, P.O. Box 43, Helsinki, FI-00014, Finland

ARTICLE INFO

Keywords:
Molecular dynamics
Tungsten
Sputtering
Fuzz

ABSTRACT

Nuclear fusion is one of the most promising concepts for future energy production, due to the almost endless source of fuel and the lack of greenhouse effects during operation. However, to successfully build a fusion reactor, the development of new materials and knowledge of their behavior are needed. One important structural part of the reactor and the reactor vessel is the wall facing the plasma. The wall will be bombarded by the products of the nuclear reaction, which will erode and degrade its performance. In this work, we study the sputtering of different tungsten surfaces under various conditions, obtaining a deeper understanding of the process using molecular dynamics simulations. Additionally, we present the evolution of W fuzz cells and the effect of surface feature height on the erosion and sputtering of the surfaces under ion irradiation.

1. Introduction

Nuclear fusion is one of the most promising sources of energy in the years to come, due to the high energy release in the nuclear reaction. The ITER experimental reactor is under construction [1–3] and it is the best candidate to study a full reactor for possible electric energy production. However, there are still several open questions related to the operation and especially to the long-term use of such a power plant, which must be answered before any commercial use. One of the still open questions is the interaction between ions and first wall materials of the reactor, which will degrade the wall and erode the material. The eroded material might then cool down the plasma. The former will decrease the up-time of the power plant, as the wall material will be hard to replace and needs a full shutdown of the power plants. The latter will in the worst case prohibit the nuclear reactions to happen at a high enough rate to be able to produce energy. The operation conditions of the future reactors [4–6] are extreme, so proper materials that can withstand these conditions are of uttermost importance. Tungsten has been chosen as the best candidate due to its good properties [7–10], such as high melting point and heavy weight, both which will reduce the sputtered and eroded amount of the wall material.

In order to understand the behavior of the wall material, there have been many studies during the last half a century on related topics, both experimental and computational. Sputtering experiments of polycrystalline materials have been studied at several different energy regimes, from hundreds of eVs up to tens of keVs [11–13]. It has been found that the ion energy, ion element and incoming angle will affect the sputtering of a certain material. In the last decades computational studies, more recently mainly molecular dynamics simulations, have been carried out from tens of eVs up to tens of keVs [14–17]. In the computational studies, similar factors as experimentally investigated have been studied, such as the effect of surface orientation on the sputtering yields. Experimentally, the effect of surface orientation has also been studied for some materials [13], but much more scarcely due to the requirement of single crystalline samples.

Investigation of the sputtering yields of different surface orientations and features are important to understand the effect of irradiation on component lifetimes. Previous studies have been utilized to understand the consequences of surface morphology on W under irradiation [18]. Jussila et al. focused on flat surfaces with random surface orientations and compared their sputtering yield with low index surface sputtering yields [19]. The erosion was found to be higher for the (100) surface from 10° to 60° at low energy compared to the other low index surfaces. These studies revealed that some small atomistic features can drastically affect the sputtering yield. Other studies have revealed the importance of cumulative impact simulations in order to obtain a quantitative agreement with experimental results of single crystalline surfaces [15,16]. In a recent article the effect of nanocolumnar tungsten surfaces on the sputtering yield was investigated both experimentally and computationally [20]. The article showed MD to be a very good tool to investigate the sputtering phenomena, and found a dramatic effect on sputtering of pillar structures compared to a flat surface. Both simulation techniques utilized, MD and BCA, showed the importance of having the correct structure, when carrying out the simulations.

Sputtering experiments of surfaces with different surface roughness showed an effect of the roughening evolution [21]. In the same study,

* Corresponding author.
E-mail address: alvaro.lopezcazalilla@helsinki.fi (A. Lopez-Cazalilla).

https://doi.org/10.1016/j.commatsci.2022.111876
Received 15 August 2022; Received in revised form 12 October 2022; Accepted 16 October 2022
Available online 29 October 2022

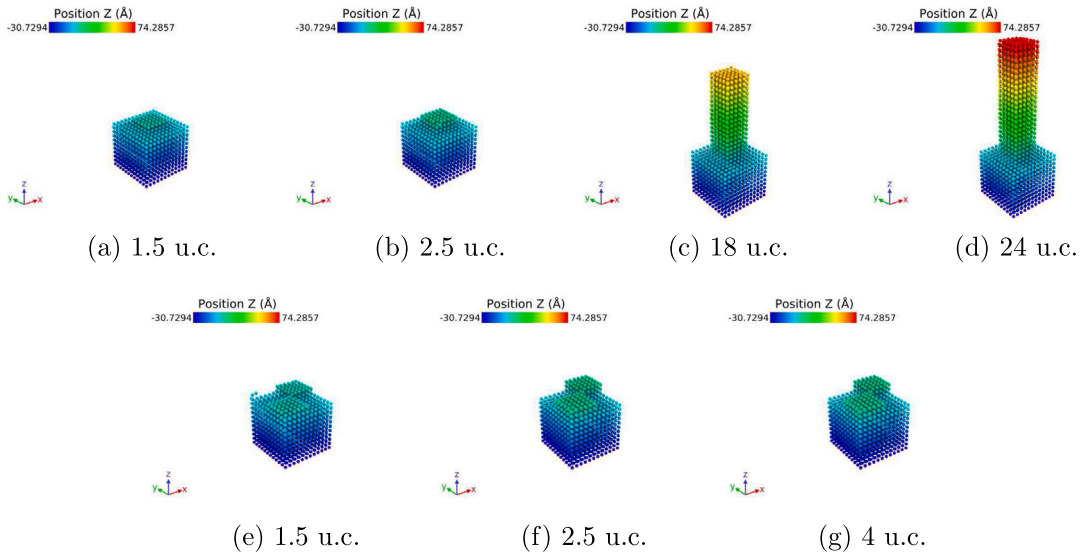

Fig. 1. Initial configuration of the two pillar configurations, for some of the investigated heights. (a)–(d) for the single pillar and (e)–(g) for the two pillars in a chess-board setup. The atoms are colored according to their heights.

simulations with a static BCA methods investigated the same surface roughness, and showed a similar effect. This reveals the importance of quantifying the different sputtering yields depending on the surface morphology [22]. In addition to the roughness as a result of manufacturing technique, several studies have shown the formation of porous parts in W under He irradiation, so-called W-Fuzz [23,24].

In this work, we study the effects of surface roughness of tungsten on the sputtering yields by 1000 eV Ar ions. Ar is one of the most used ions in experimental sputtering studies and is also used as a seeding gas in the future fusion reactors [25,26]. We investigated the (100) surface and surface structures of this orientation to see the effects of only the morphology.. Low and medium energy irradiation was conducted at different incoming angles to study the implications. To understand the underlying mechanisms, we have investigated different surface structures and features to study the sputtering phenomena of them. We found the sputtering to be affected by different features in different manner, and also an effect of the height of the features. An effect of different incoming angles was also observed.

2. Methods

2.1. Molecular dynamic simulations

The simulations were carried out with the PARCAS MD code [27]. Periodic boundary conditions were applied in the x- and *y*-directions. The surface in the *z*-direction was open and oriented as a (100) surface. The simulations were carried out at 300 K, utilizing three different zones. At the bottom a few layers (about 6 Å) of atoms were fixed to prevent the cell from moving. Above the fixed atoms a few layers of atoms (about 10 Å) were thermally controlled by a Berendsen thermostat [28] to keep the temperature constant. All the rest of the atoms followed a NVE ensemble.

The interactions between the W atoms was described using the Marinica potential [29] with the corrections by Sand et al. [30], and the Ar-W and Ar-Ar interactions were defined by the DMol potential [31]. Electronic stopping power was considered for all atoms with a kinetic energy more than 10 eV. The incoming ion was always initiated 6 Å over the highest of point of cell. The azimuthal angle was always fixed and we investigated several irradiation angles, from normal incidence to grazing incidence.

We performed two kinds of simulations from the point of view of the irradiation method: single-impact [19] and sequential-impacts [32,33]. In single-impact simulations, between 1200 and 10 000 impacts at random initial positions were carried out for statistics. In the sequential-impacts, between 2000 and 5000 impacts were carried out in the same cell, enough to study the evolution of the surface under prolonged irradiation. In order to randomize the impact position, the cells were shifted randomly in the two periodic directions, so that the ion always was directed towards the center of the top surface.

As a reference surface for our different surface morphologies, we used the (100) surface. These results have been obtained previously under identical circumstances in Ref. [20], both for single and sequential impact.

2.2. Simulation cell creation

2.2.1. Pillars

To observe the effects of height and shape of a structure in the single-impact simulations, we constructed different cells to perform the irradiation on. These cells were constructed from a (100) surface and they have two main configurations:

- one pillar in the center of the cell, with the x- and y-dimensions half of that of the bottom box
- two pillars mimicking a chessboard, where each of the pillars had the x- and y-dimensions half of the bottom box

Both setups were studied utilizing different heights (in units of unit cells (u.c.) over the initial surface), in total 7 and 5, for the two setups, respectively. The single pillar covers 25% and the two pillars in the chess-board setup covers in total 50% of the bottom box. The cells were periodic in x- and *y*-directions, mimicking a period structure.

Fig. 1 shows some of the cells used in this part of the work. We used 100 and 200 eV Ar irradiation under 0°, 30°, 60° and 80° incoming angles. The simulation time was 10 ps for each individual impact and 10 000 impact were carried out for each case. In order to select the random impact point, we randomly shifted the cell over the periodic boundaries, and the ion was directed towards the center of the cell aligned with the *x*-direction. This method allows to pin-point the effects of different surface feature heights on the sputtering yields.

2.2.2. W fuzz

Crowson et al. [34,35] developed a method to create a foam structure with porosity $p = 0.5$ by a spinoidal decomposition of a Au-based binary alloy. This method was applied to study the sputtering of

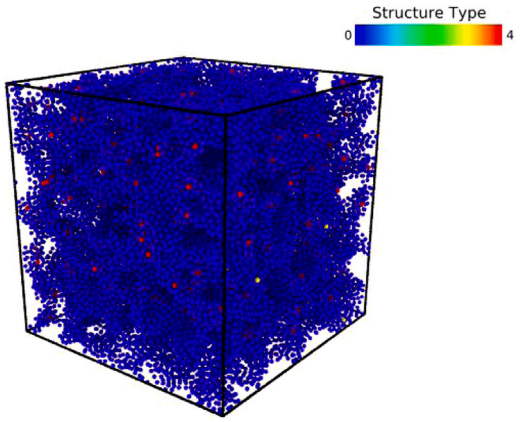

Fig. 2. Amorphous structure after annealing at 300 K.

nanoporous materials [36]. In our case to perform the spinoidal decomposition to study the effect of porosity in W, we only consider one element, and to create the fuzz following the same method, and instead of having a second element, we remove one atom per created cell in the BCC structure. Hence, the process is as follows: we create a single crystal structure with the correct lattice constant at 300 K. Then, we remove the central atoms of every unit cell and the structure is annealed at 300 K for 50 ps. This process left several tunnels in the material (see Fig. 2). Next, the created fuzz, is placed on the (100)-oriented substrate and, during this step, the structure reorganizes during the relaxation done at 300 K for 100 ps. Doing this, we generate the structure with a porosity of about 50%.

In the case of sequential sputtering, once the fuzz is created, it is placed on top of a (100) surface, and then the structure is relaxed at 300 K. The final configuration after placing 4 identical fuzz structures on the surface is shown in Fig. 3. In this case, the simulation time was 12 ps per impact, where the first 10 ps were following the NVE ensemble and a thermal bath at the bottom layers, and during the last 2 ps the cell was thermalized by a thermostat on all atoms, to avoid temperature build-up throughout the sequential irradiation. After thermalization a new impact was started, and the same procedure was carried out to observe the effect of cumulative impacts. We simulated 2500 impacts for 1000 eV at 0°, 25°, 45°, 60°, 70°, 80° and 85° off-normal.

For single-impact irradiation, we applied the same methodology for creating the cell, however, instead of four fuzz structures, we placed one single fuzz structure on top of a pristine W structure of the same size. This setup was simulated for 1200 Ar impacts at normal incidence at the energies 100 eV, 200 eV, 500 eV and 1000 eV.

2.2.3. Hemi-ellipsoid

Hemi-ellipsoids of different heights were constructed out of a single-crystalline W BCC box and relaxed, in order to obtain a representative surface of the ellipsoid. In the work developed by Arredondo et al. [21], it was observed different surface roughnesses on W, varying from a few nm (*smooth*) to hundreds of nm (*rough*), affected the sputtering. In order to compare with these experiments and BCA simulations, we chose to recreate the *smooth* case, which can be accurately be reproduced in full molecular dynamics simulations. In subfigures (a) of Figs. 11, 12 and 13, the three different configurations studied are shown. We investigated features with similar size in two dimensions but different in the height dimension (z-direction), which will both yield a different aspect ratio as well as a different shape. We study three cases (heights): 3, 4 and 6 nm. The irradiation is done sequentially along the y-axis in this study. The simulation time was 12 ps per impact (the first 10 ps were following the NVE ensemble and thermally controlling a few bottom layers of atoms, and during the last 2 ps the cell was thermalized with a thermostat on all atoms in order to restore the temperature to 300 K after the impact). We performed simulations using 1000 eV Ar at 0°, 25°, 45°, 60°, 70°, 80° and 85°.

2.2.4. Analysis

To obtain the sputtering yield, we consider atoms as sputtered if they are located further than 5 Åabove the surface (z direction). We collect the number of sputtered atoms and the initial position of these atoms. From the former, we obtain the average sputtering yield, and this is calculated for all the simulation setups. In the case of single-impact simulations, we also get the standard error of the mean (σ_x) as

$$\sigma_x = \frac{\sqrt{\sum_{i=1}^{N} \frac{1}{N}(\bar{x} - x_i)^2}}{\sqrt{N}}, \tag{1}$$

where N is the number of impacts and $\bar{x}$ is the sputtered atoms mean of the N cases.

For the case of pillars described in Section 2.2.1, we analyze the initial position of the sputtered atoms and calculate the frequency of sputtering for each atom. This information is used to create histograms in order to identify which atoms are sputtered, and therefore can reveal insights in the sputtering phenomena.

3. Results & discussion

3.1. Single-impact simulations

In this section we present the results obtained from all the single-ion impact simulations for all investigated setups. The results are focusing on the effect of fuzz versus a pristine surface and on the effect of the height of surface features.

3.1.1. Fuzz vs Flat

The results of single impacts on the fuzz structures compared to a pristine (100) surface is shown in Fig. 4. We observe how the sputtering yield is higher for the flat surface compared to the fuzz structure. In both cases, the sputtering yield increases as the incident ion energy increases. The lower sputtering yield of the fuzz structure reveals that once the fuzz on the surface is created, the sputtered atoms can be redeposited inside the structure instead of sputtering away. As, even though sputtering might happen, if the initial position of the atom was not in one of the top most layers i.e. the ion travels through the created tunnels, the sputtering will happen deep inside the material. This shows that there is an effect of the tunnels and the irregularities on the surface on the final result of sputtering.

In the work by Nakamura et al. [22], the authors performed Binary Collision Approximation (BCA) simulations of Ar at normal incidence for several energies on (100) W surfaces, among others. We see that our results are considerably lower than the ones obtained using BCA in Ref. [22]. BCA is heavily influenced by the parametrization used for the particular case, and at low energies BCA has been seen to overestimate the results [14,38].

3.1.2. Pillars: Different heights and configurations

In Fig. 5 the sputtering yield for all heights and both setups are shown. In Fig. 5(a) the single pillar results are visualized and in Fig. 5(b) the chessboard structure. Overall, the results at 100 eV are lower than at 200 eV, as expected. Observing the single-pillar results, Fig. 5(a), at normal incidence for 100 eV, the maximum is obtained for the flat surface structure. The trend is that the higher the structure is, the lower the sputtering yield is (see also Fig. 6). This is more obvious at 30° off-normal, where the lowest sputtering yields are for the two highest structures (18 and 24 unit cells high pillars). At 60° and 80°, the discrepancies between the different heights decrease. However, looking at the flat surface result, we observe how at 60° and 80°, the sputtering yield decreases to zero. On the other hand, if we pay attention to the 200 eV results, in general the maximum for the lower structures is located at 30°, but at 60° for the higher structures. We observe a great difference at normal incidence between the lower and higher structures,

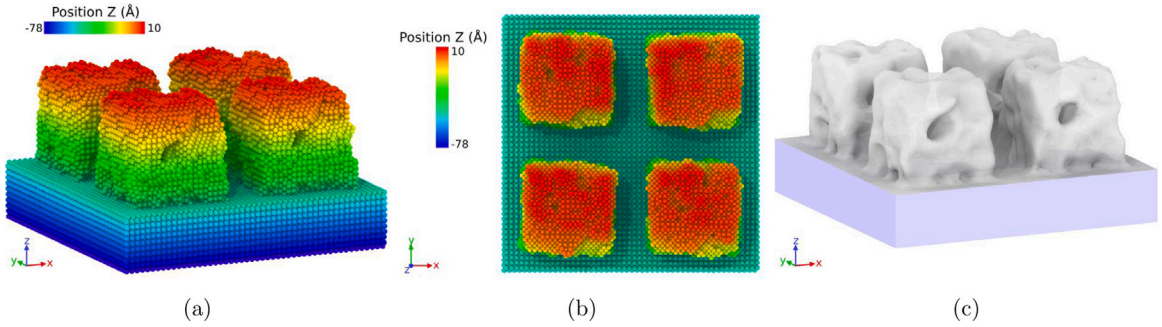

Fig. 3. Final configuration after relaxation of the fuzz structure from a perspective view (a), from the top (b) and (c) showing the surface mesh created using OVITO [37].

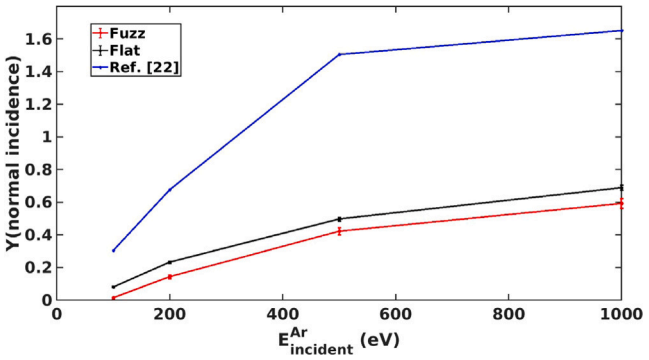

Fig. 4. Sputtering yield as a function of the ion energy at normal incidence using single impact for the fuzz structure compared to a flat surface. The results are compared with the sputtering yield for a (100) W surface extracted from Ref. [22].

however this difference decreases at grazing incidence. In the case of 18 and 24 u.c. high pillars, the sputtering yield at higher incidence angles is greater than at lower incidence angles. In this case, again, sputtering at close-to-normal incidence is higher for the flat surface, but it gradually decreases at 60°, and then, to zero at 80°.

Looking at Fig. 5(b), the chessboard structures, we can observe that for 100 eV the incoming angle does almost not at all affect the sputtering yield, except at the largest incoming angle. At 200 eV, we see an increase in sputtering yield as the incoming angle increases, with the maximum at 60°. Similarly to the single pillars, a high sputtering yield at the largest incoming angles for the chessboard, where at the same incoming angle a flat surface has almost zero sputtering yield.

If we compare the two kinds of structures (Fig. 5(a) and (b)), we observe that in the case of the chessboard structure, the sputtering yield is in general higher than for the single pillar. In order to investigate deeper differences, we calculate histograms on the frequency of the atoms being sputtered. Here, we present normal incidence and 60° at 100 eV (for all the other angles and energies, the histograms are found in the Supplementary material online, see Sec. S1). In Fig. 7 we see the differences between the surfaces simulated. We clearly observe how for low structures, Fig. 7(a), (b), (h) and (m), both the bottom surface and the surface of the pillars are sputtered. While for the higher features, Fig. 7 (c), (d), (e), (f), (g), (h), (j), (k) and (l), the bottom surfaces remain almost intact. We observe how the bottom surface will not sputter practically at all when the pillars are high enough. However, it needs to be noted, that we analyze the complete sputtering, e.g. atoms from the bottom surface may be sputtered, however, they are redeposited at the pillar, leading to no sputtering. This same trend is seen for 200 eV energies also, with more sputtering from the bottom surface observed at higher pillars.

Looking at similar histograms, but at an incoming angle of 60°, we can see drastic changes in the behavior (Fig. 8). At the higher incoming angles, in principle only the atoms on the ledge of the pillars are sputtered away. Therefore, as seen in the overall sputtering yields, the height does not affect the sputtering at all at these large incoming angles. This ledge explains why the pillars and chessboard structures show a high sputtering yield, whereas a flat surface show almost none, similarly as seen previously in Ref. [19] for random surface orientations.

In order to explain the seen mechanisms behind sputtering, we can observe:

- The higher the feature is, the lower the sputtering yield is at normal incidence. This can be explained by the sputtering exclusively happening at the top surface of the pillar/feature. We can clearly see that the sputtering yield will drop to about 25% in the pillar case and to about 50% of the flat surface, when the features are high (see Fig. 6). These numbers are the fraction of the top area compared with the total area of the cell. It will go even below this fraction, due to the edge atoms are more likely to sputter downwards and get redeposited, than to sputter upwards.
- At large incoming angles we can see that sputtering happens almost exclusively at the ledges of the features. Therefore, it can be observed that the chessboard with effectively double the ledge-length will yield a two-fold sputtering yield compared to the single pillar.

3.2. Sequential-impacts simulations

In the sequential-impact simulations, we first focus on the individual setups, and both track the evolution of the surface under prolonged irradiation and compare similar setups to each other, where applicable. In the last sub-section, all results from the sequential-impact simulations are compared to each other in order to see the relative effects of different features. The evolution of a single surface or surface structure will give great insight in the sputtering phenomena and the relative effects of different features on the total sputtering yield will help us explain the experimentally seen trends.

3.2.1. Flat (100) surface

The evolution of the flat (100) surface under sequential 1000 eV irradiation is followed in Fig. 9. In the figure, the final configuration of the (100) surface under different irradiation angles after 5000 impacts is presented. Looking at how the surface is affected differently at different incoming angles, we observe that the surface roughens in all cases but at grazing incidence (Fig. 9(d)), where the surface remains intact. In Fig. 9(a) we notice the effect of the normal incidence ions, creating surface defects, however this effect increases at higher inclinations. We observe that at 30° and 60° (Fig. 9(b) and (c)) the surface is more rough than at 0° (Fig. 9(a)). At 85°, the surface remains intact. This surface arrangement can be explained by the higher sputtering yield at 30° – 70° and lower at grazing incidence, compared to normal incidence, seen in Fig. 10.

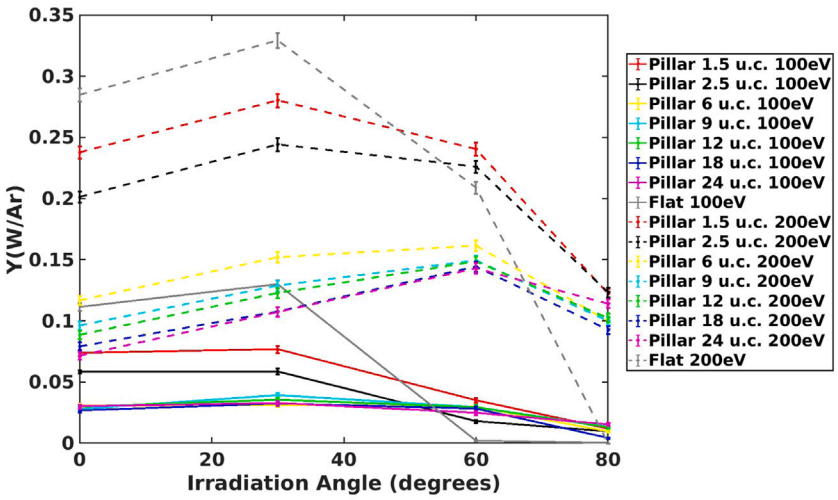

(a) Pillar

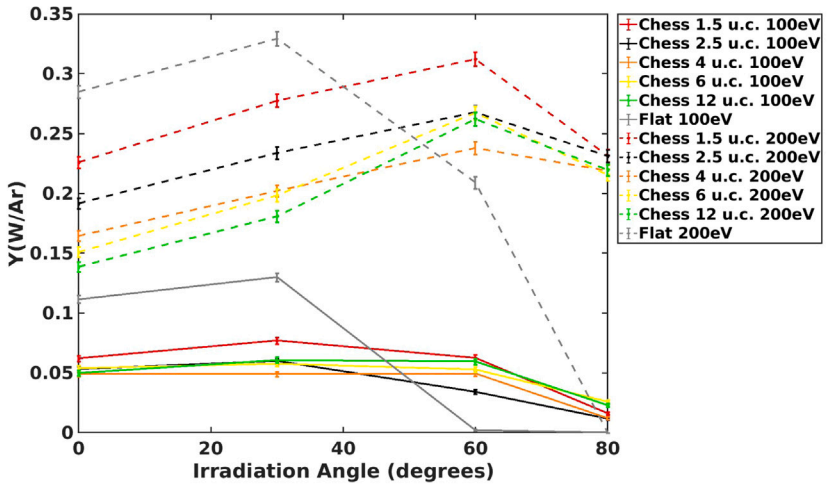

(b) Chessboard

Fig. 5. Sputtering yield for the pillars (a) and chessboard (b) structure compared to the flat ones.

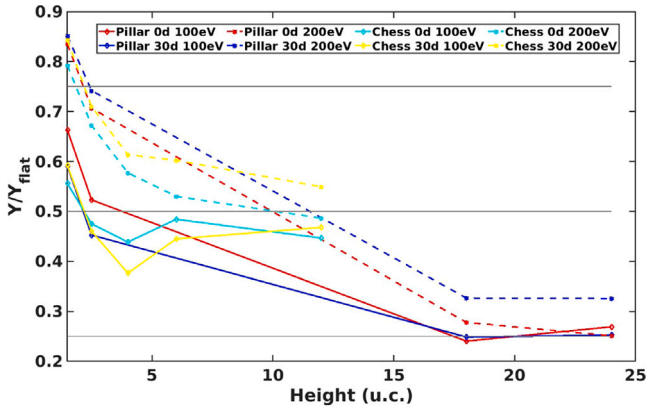

Fig. 6. Sputtering yields for the pillars and chessboard structures at 0° and 30°, divided by the sputtering yield for the flat surface at the same irradiation angles, as a function of the height of the pillars. The gray lines mark the 25%, 50% and 75% of the value.

In Fig. 10, we clearly see that the sputtering yield is greater at 30° than at normal incidence, showing that at the latter, the irradiation can increase the roughness of the surfaces, but the atoms on the surface does not leave it. The maximum sputtering yield is obtained at 45° off-normal. We can also notice that the sputtering yield at 80° drops to zero, showing that more cases would be needed to remove an atom from the surface at this energy-inclination combination. The sequential-impacts scheme has been applied previously in other cases for different materials [20,32,33]. It was observed that in metals, higher irradiation energy is needed to erode atoms at grazing incidence, otherwise the probability of the ion to be reflected is very high. This explain the drop of sputtering at high angles shown in Fig. 10.

3.2.2. *Hemi-ellipsoid*

The final surface structures after 5000 impacts at 1000 eV for all three investigated heights of the hemi-ellipsoid can be found in Figs. 11–13 (and in the Supplementary material in Figs. S7–Figs. S9). Looking at the 3 nm-high structure, Fig. 11, we observe the clear effect of the consecutive irradiation of the surface in all the cases, however, at the incoming angles of 45°, 60° and 70° the effects are more noticeable. In these cases the protrusions have almost vanished from the surface. On a general level the mound in front of the hill is not high enough to survive up to this fluence at any of the incoming angles.

For the 4 nm-high structure, Fig. 12, we observe that the structure is less damaged than in the 3 nm case. This is especially clear at normal incidence and 85° (Fig. 12(b) and (e)). We also notice that the incoming ions have a particular effect eroding atoms in base of the mound, more remarkable at 45° (Fig. 12(c)).

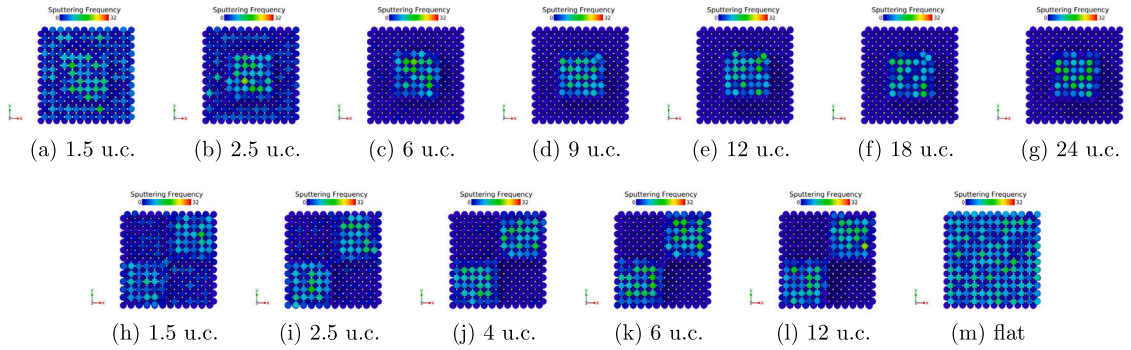

Fig. 7. Sputtering frequency at 100 eV and normal incidence for a pillar in the center, (a)–(g), and for two pillars, (h)–(l), and flat, (m) (The atoms are colored according to their sputtering frequency).

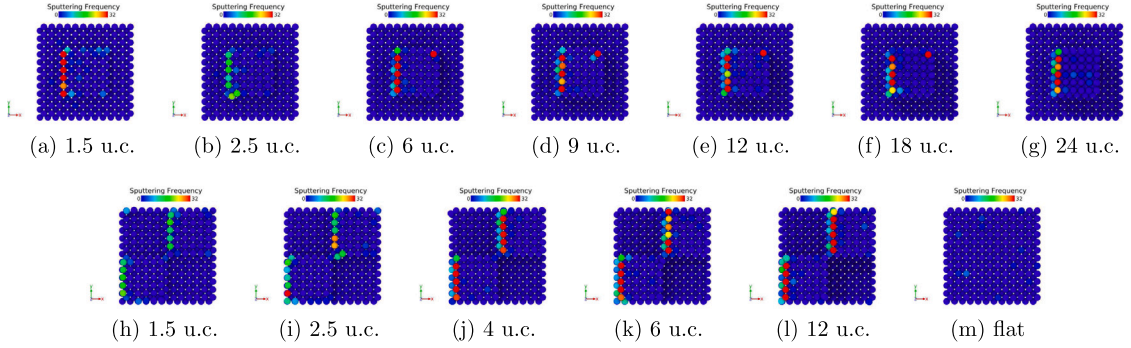

Fig. 8. Sputtering frequency at 100 eV and 60° for a pillar in the center, (a)–(g), and for two pillars, (h)–(l), and flat, (m), (The atoms are colored according to their sputtering frequency).

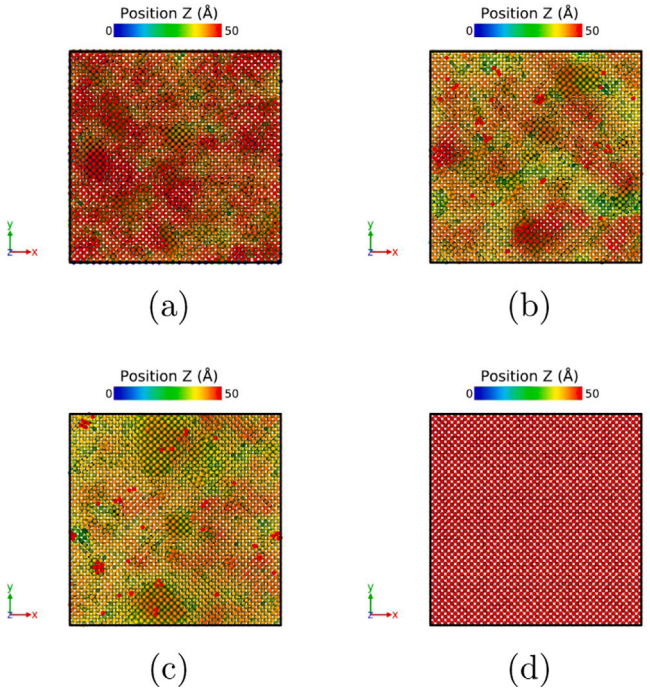

Fig. 9. Top surface of the flat cell after 5000 impacts of 1000 eV at (a) 0°, (b) 30°, (c) 60° and (d) 85° incoming angle.

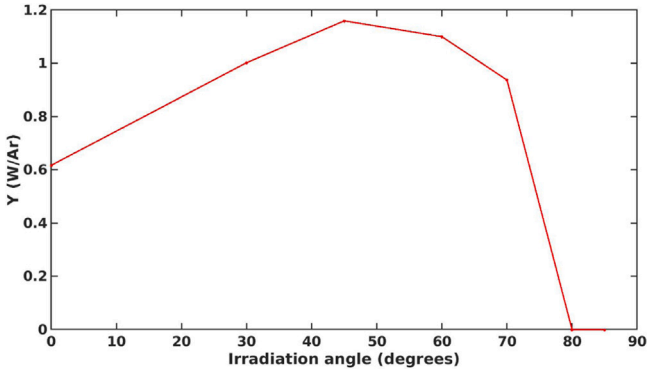

Fig. 10. Sputtering yield as a function of the irradiation angle for the flat surface at 1000 eV (averaged over 5000 impacts). The results are a continuation of the flat surface results shown in Ref. [20] up to 5000 impacts.

Looking the 6 nm-high structure, Fig. 13, we observe that the trends are similar to the previous two cases: the structures still remain clearly visible the surface after the 5000 impacts in almost all cases, however, the pit created in the base of the mound is more visible than in the 4 nm case (see Fig. 13(b)–(d)). We see that in the cases of 45° and 60° (Fig. 13(c) and (d), respectively) the top of the hemi-ellipsoid has decreased more than for the other incoming angles. On the other hand, the 85° (Fig. 13(e)) the protrusion is almost unchanged, with only some minor observable surface changes.

In order to investigate the reason for the slightly different behavior for the different heights, we look at the averaged sputtering yield over the 5000 impacts, Fig. 14. We can observe the following three trends:

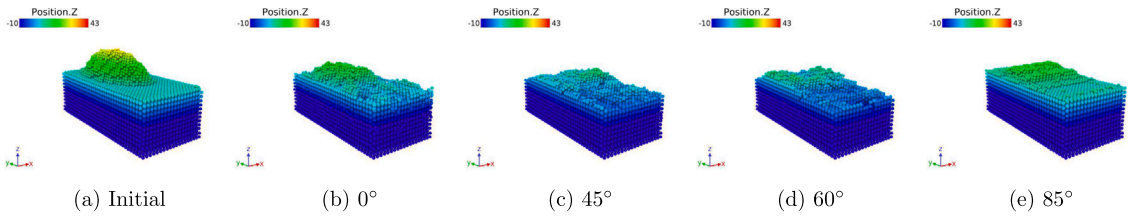

Fig. 11. Initial surface of the 3 nm high hemi-ellipsoidal, (a), and after 5000 impacts at 1000 eV each at different incoming angles, (b)–(e).

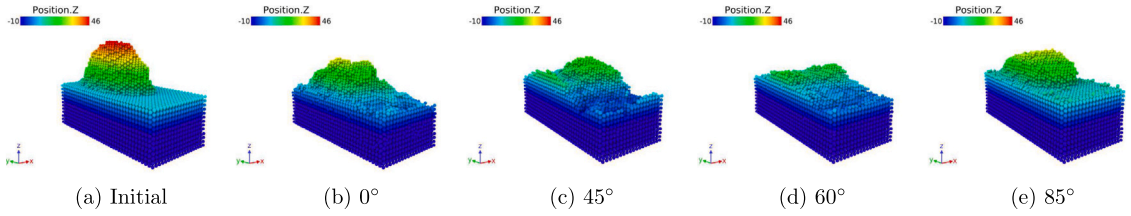

Fig. 12. Initial surface of the 4 nm high hemi-ellipsoidal, (a), and after 5000 impacts at 1000 eV each at different incoming angles, (b)–(e).

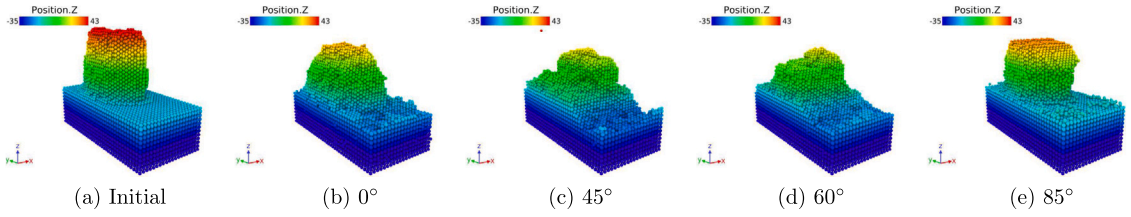

Fig. 13. Initial surface of the 6 nm high hemi-ellipsoidal, (a), and after 5000 impacts at 1000 eV each at different incoming angles, (b)–(e).

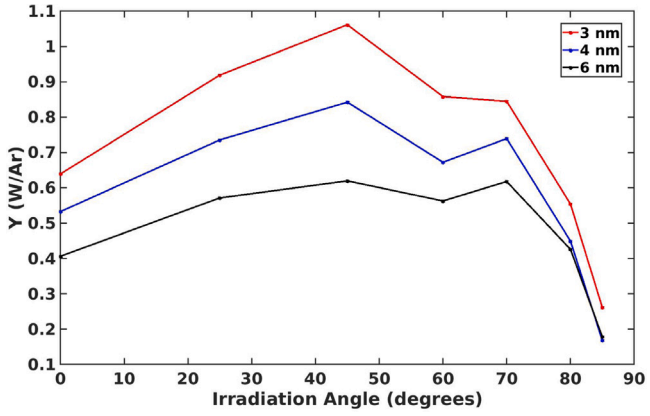

Fig. 14. Sputtering yield as a function of the irradiation angle for the hemi-ellipsoidal surfaces at 1000 eV (averaged over 5000 impacts).

- The higher the structure, the lower the sputtering yield.
- The maximum sputtering is happening at 45°, with a second peak at 70° (as important as the first peak for the highest structure, 6 nm).
- The lower the structure is, the more important the role the incoming angle plays.

3.2.3. Fuzz surface

In Fig. 15, the irradiated fuzz structures after 2500 impacts are shown for 1000 eV incoming ion energy. We notice that, with the exception of 85°, the surfaces have been modified due to irradiation. In the simulations of low incoming angles, we observe a clear modification of the surface, however, the sputtering yield is lower than at greater incoming angles (see Fig. 16). The cases at 60° and 70° are the most damaged, as we can see in Fig. 15(d) and (e), respectively.

In Fig. 16, we see the sputtering yield as a function of the irradiation angle for 1000 eV. We notice that the sputtering yield increases up to 45°, where the maximum of sputtering is obtained. Then, it plateaus out up to 70°, to decrease after that point down to the minimum value.

3.3. Effect of surface morphology differences

Combining the results obtained in the previous subsections, we can get a more clear picture of the effect of surface morphology on the sputtering yield. Considering the sequential results at the ion energy 1000 eV for all setups, we get the results shown in Fig. 17.

We observe that the sputtering yield for the flat surface is in general (angles up to 60°) higher at all angles and, furthermore, the change in the surface profile suppresses the erosion in general. As we anticipated before, in the case of the hemi-ellipsoidal shape, the height of the structure is playing a crucial role preventing the atoms to be sputtered. The fuzz with similar height as the 6 nm hemi-ellipsoid show a very similar trend as the hemi-ellipsoid. It has been previously observed that this kind of surface roughness can reduce the sputtering drastically, although on a larger scale [21].

Additionally, the curvature of the structure is an important factor, as the local irradiation angle i.e. the angle between the ion and the local surface angle compared to a flat one, can be very different from the incoming angle. We see that at lower inclinations, the fuzz and the 6 nm-high hemi-ellipsoidal structure results are quite alike. However at grazing incidence, we see a larger drop in the sputtering for the flat and the fuzz structure compared to the hills. At those irradiation angles, it is harder to remove atoms from the surface in these two cases, however the slopes in the hemi-ellipsoidal structures enhance the probability of eroding atoms. This effect is mainly due to the exact location of the impact point, which most likely decreases the local incidence angle between the ion and the local surface. In the fuzz case, we observed that

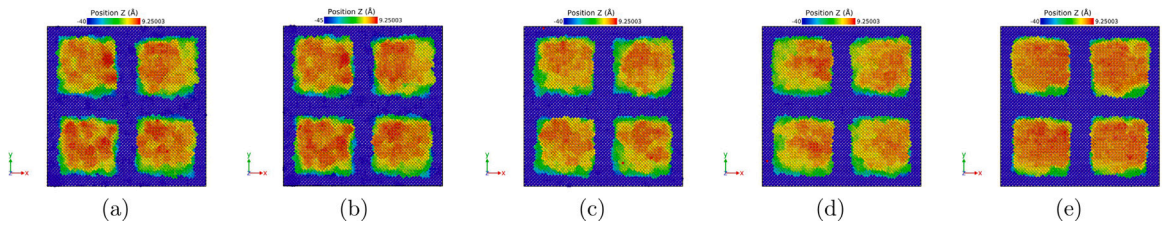

Fig. 15. Top surface of the fuzz cell for 1000 eV at (a) 0°, (b) 45°, (c) 60°, (d) 70° and (e) 85°, after 2500 impacts.

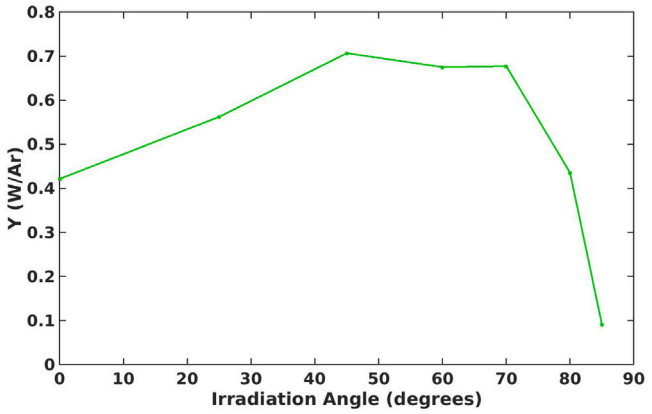

Fig. 16. Sputtering yield as a function of the irradiation angle for the fuzz at 1000 eV (averaged over 2500 impacts).

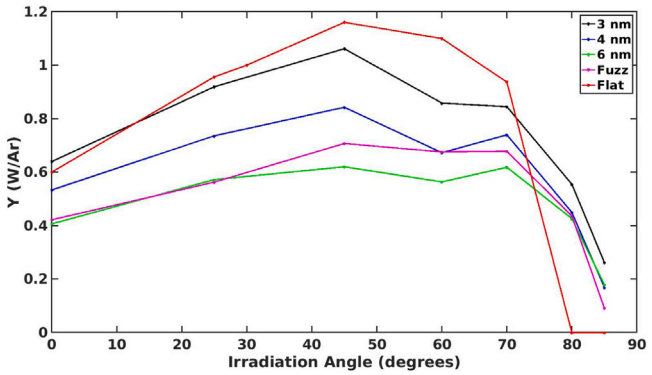

Fig. 17. Sputtering yield for all the surfaces in the sequential mode.

the ions can be trapped inside the structures and if it hits inside one of the tunnels, being sufficiently energetic, it can erode atoms inside the tunnels. However, these initially-sputtered atoms, are redeposited again in the cell, resulting in a net-zero sputtering.

We can see in Fig. 17 how the morphology of the surface is affecting the erosion of them. We see how the flat surfaces enhance the sputtering yield at angles off-normal mainly until grazing incidence, where the number of sputtered atoms decrease considerably. The effect of the height in the hemi-ellipsoidal structure is crucial for suppressing the erosion in the surface. This fact is also noticed in the single-impact simulations, where the effect of the height in the pillar and chessboard structures is similar as in the hemi-ellipsoidal structures. We see that regardless the height of the pillars, the erosion is lower than in the flat case at small irradiation angles, however at higher angles, the effect is the opposite (Fig. 5). At normal incidence, at various energies, we also observed that the fuzz surface decreases the erosion compared to the flat case.

In this study we have thoroughly studied the effect of 1000 eV Ar ions impacting on (100) surfaces and surface structures with this orientation. The general trends, like the mechanisms for downward sputtering and sticking are most likely also seen for other surface orientations, ion energies and ion species. The erosion trends seen for different hills should also be similar. Going to very high energies or light ions where the penetration depth of the ion is large, the results will most likely be affected by the lack of energy deposited in the surface layers. Again going to very low energies, the sputtering event is mainly governed by the exact atomistic configuration and impacts point, which might also affect the results.

4. Conclusions

In this work, we have studied the effect of different surface morphologies on the sputtering of W surfaces. The different morphologies spanned from surface features seen experimentally to more well-defined simple geometries, in order to understand the sputtering phenomena on a deeper level. Both single and sequential impacts were simulated, the latter to study the morphology change under continuous irradiation.

- The introduction of W fuzz and other structures to MD allowed us to understand how it behaves under ion irradiation, knowing that it plays a role in the durability of plasma-facing materials. We know that surface structures exist and that fuzz structures are formed in W [23,24]. With this method we can study how they influence the sputtering. Comparing the results with the ones of a flat surface at different energies, we see how the increase of the roughness of the surfaces modify the behavior of the material under irradiation.
- The single-ion studies are a fast way to know the response of the different configurations and compare their results and fair statistics using small cells can be obtained. We measured the sputtering yield of the fuzz structure at different energies, showing that the erosion is lower for the fuzz compared to a flat surface.
- The pillars and chessboard-like structures provide good information on how the surface modification influences the sputtering phenomena. We studied the importance of atom position on the surface in relation to their probabilities of being sputtered. When the aspect ratio goes up, sputtering is only observed from the top of the features, leading to a lowering of the sputtering yield. This sputtering yield is in direct correlation with the relative size of the top surface compared to the total surface.
- The sequential irradiation of the samples provide a more detailed view of the sputtering process. The results shows that when the roughness of a surface (height of a structure) increase, the sputtering yield decreases along all the irradiation angles domain. The only exception is at grazing incident, where the more rough surfaces show a higher sputtering yield than the flat ones.
- All the results included in this work contribute to the creation of a more realistic picture of the erosion of W, under different circumstances. When the ions impact the material, they change the local atomic configuration, which shows the importance of sequential sputtering simulations. Utilizing these results, we can obtain a better estimation of the sputtering of surfaces under fusion conditions.

CRediT authorship contribution statement

Alvaro Lopez-Cazalilla: Writing – original draft, Writing – review & editing, Methodology, Investigation. **Joonas Jussila:** Methodology. **Kai Nordlund:** Project administration, Investigation, Resources. **Fredric Granberg:** Supervision, Writing – review & editing, Investigation.

Declaration of competing interest

The authors declare that they have no known competing financial interests or personal relationships that could have appeared to influence the work reported in this paper.

Data availability

Data will be made available on request.

Acknowledgments

This work has been carried out within the framework of the EUROfusion Consortium and has received funding from the Euratom research and training programme 2014–2018 and 2019–2020 under grant agreement No 633053. This work has been carried out within the framework of the EUROfusion Consortium, funded by the European Union via the Euratom Research and Training Programme (Grant Agreement No 101052200 — EUROfusion). Views and opinions expressed are however those of the author(s) only and do not necessarily reflect those of the European Union or the European Commission. Neither the European Union nor the European Commission can be held responsible for them. Computer time granted by the IT Center for Science – CSC – Finland and the Finnish Grid and Cloud Infrastructure (persistent identifier urn:nbn:fi:research-infras-2016072533) is gratefully acknowledged.

Appendix A. Supplementary data

Supplementary material related to this article can be found online at https://doi.org/10.1016/j.commatsci.2022.111876.

References

[1] ITER Physics Basis Editors ITER Physics Expert Group Chairs and Co-Chairs and ITER Joint Central Team and Physics Integration Unit, ITER physics basis, Nucl. Fusion 39 (12) (1999).
[2] Progress in the ITER physics basis editors, Progress in the ITER physics basis, Nucl. Fusion 39 (12) (2007).
[3] J. Wesson, Tokamaks, Second Oxford Engineering Series, Clarendon Press, Oxford, 1997.
[4] Y. Ueda, J. Coenen, G.D. Temmerman, R. Doerner, V.P.J. Linke, E. Tsitrone, Research status and issues of tungsten plasma facing materials for ITER and beyond, Fusion Eng. Des. 89 (7) (2014) 901–906.
[5] J. Knaster, A. Moeslang, T. Muroga, Materials research for fusion, Nat. Phys. 12 (2016) 424–434.
[6] V.P. Budaev, Results of high heat flux tests of tungsten divertor targets under plasma heat loads expected in ITER and tokamaks (review), Z. Phys. 79 (2016) 1137–1162.
[7] V. Barabash, G. Federici, R. Matera, A.R. Raffray, I.H. Teams, Armour materials for the ITER plasma facing components, Phys. Scr. 74 (1999) 1999.
[8] R. Nygren, R. Raffray, D. Whyte, M. Urickson, M. Baldwin, L. Snead, Making tungsten work - ICFRM-14 session T26 paper 501 nygren, others, making tungsten work, J. Nucl. Mater. 417 (2011) 451–456.
[9] J. Alvarez, D. Garoz, R. Gonzalez-Arrabal, A. Rivera, M. Perlado, The role of spatial and temporal radiation deposition in inertial fusion chambers: The case of HiPER, Nucl. Fusion 51 (2011) 053019.
[10] M. Kaufmann, R. Neu, Tungsten as first wall material in fusion devices, Fusion Eng. Des. 82 (2007) 521–527.
[11] W. Eckstein, Sputtering yields, in: Sputtering By Particle Bombardment, in: Topics in Applied Physics, Springer, Berlin, Heidelberg, 2007, p. 110.
[12] Y. Stark, R. Frömter, D. Stickler, H. Oepen, Sputter yields of single- and polycrystalline metals for application in focused ion beam technology, J. Appl. Phys. 105 (2009) 013542.
[13] T. Nagasaki, H. Hirai, M. Yoshino, T. Yamada, Crystallographic orientation dependence of the sputtering yields of nickel and copper for 4-keV argon ions determined using polycrystalline targets, Nucl. Instrum. Methods Phys. Res. B 418 (2017) 34–40.
[14] A. Lopez-Cazalilla, A. Ilinov, L. Bukonte, F. Djurabekova, K. Nordlund, S. Norris, J. Perkinson, Simulation of atomic redistribution effects in a-Si under ion irradiation, Nucl. Instrum. Methods Phys. Res. B 414 (2018) 133–140.
[15] A. Lopez-Cazalilla, D. Chowdhury, A. Ilinov, S. Mondal, P. Barman, S.R. Bhattacharyya, D. Ghose, F. Djurabekova, K. Nordlund, S. Norris, Pattern formation on ion-irradiated Si surface at energies where sputtering is negligible, J. Appl. Phys. 123 (2018) 235108.
[16] F. Granberg, A. Litnovsky, K. Nordlund, Low energy sputtering of Mo surfaces, J. Nucl. Mater. 539 (2020) 152274.
[17] E.A. Hodille, J. Byggmästar, E. Safi, K. Nordlund, Sputtering of beryllium oxide by deuterium at various temperatures simulated with molecular dynamics, Phys. Scr. 2020 (2020) 014024.
[18] E. Marenkov, K. Nordlund, I. Sorokin, A. Eksaeva, K. Gutorov, J. Jussila, F. Granberg, D. Borodin, Angular and velocity distributions of tungsten sputtered by low energy argon ions, J. Nucl. Mater. 496 (2017) 18–23.
[19] J. Jussila, F. Granberg, K. Nordlund, Effect of random surface orientation on W sputtering yields, Nucl. Mater. Energy 17 (2018) 113–122.
[20] A. Lopez-Cazalilla, C. Cupak, M. Fellinger, F. Granberg, P.S. Szabo, A. Mutzke, K. Nordlund, F. Aumayr, R. González-Arrabal, Comparative study regarding the sputtering yield of nanocolumnar tungsten surfaces under Ar^+ irradiation, Phys. Rev. Mater. 6 (2022) 075402.
[21] R. Arredondo, M. Oberkofler, T. Schwarz-Selinger, U. von Toussaint, V. Burwitz, A. Mutzke, E. Vassallo, M. Pedroni, Angle-dependent sputter yield measurements of keV D ions on W and Fe and comparison with SDTrimSP and SDTrimSP-3D, Nucl. Mater. Energy 18 (2019) 72–76.
[22] H. Nakamura, S. Saito, A.M. Ito, Sputtering yield of noble gas irradiation onto tungsten surface, J. Adv. Simul. Sci. Eng. 3 (2017) 165–172.
[23] S. Kajita, S. Kawaguchi, N.Y N. Ohno, Enhanced growth of large-scale nanostructures with metallic ion precipitation in helium plasmas, Sci. Rep. 8 (2018) 56.
[24] S. Kajita, N. Yoshida, N. Ohno, Tungsten fuzz: Deposition effects and influence to fusion devices, Nucl. Mater. Energy 25 (2020) 100828.
[25] A. Kallenbach, M. Bernert, R. Dux, L. Casali, T. Eich, L. Giannone, A. Herrmann, R. McDermott, A. Mlynek, H.W. Müller, F. Reimold, J. Schweinzer, M. Sertoli, G. Tardini, W. Treutterer, E. Viezzer, R. Wenninger, M. Wischmeier, the ASDEX Upgrade Team, Impurity seeding for Tokamak power exhaust: From present devices via ITER to DEMO, Plasma Phys. Control. Fusion 55 (2013) 124041.
[26] H. Urano, M. Nakata, N. Aiba, H. Kubo, M. Honda, N. Hayashi, M. Yoshida, Y. Kamada, the JT-60 Team, Roles of argon seeding in energy confinement and pedestal structure in JT-60U, Nucl. Fusion 55 (2015) 033010.
[27] K. Nordlund, Molecular dynamics simulation of ion ranges in the 1-100 keV energy range, Comput. Mater. Sci. 3 (4) (1995) 448–456.
[28] H.J.C. Berendsen, J.P.M. Postma, W.F. van Gunsteren, A. DiNola, J.R. Haak, Molecular dynamics with coupling to an external bath, J. Chem. Phys. 81 (8) (1984) 3684–3690.
[29] M.C. Marinica, L. Ventelon, M.R. Gilbert, L. Proville, S.L. Dudarev, J. Marian, G. Bencteux, F. Willaime, Interatomic potentials for modelling radiation defects and dislocations in tungsten, J. Phys. 25 (39) (2013) 395502.
[30] A.E. Sand, et al., Non-equilibrium properties of interatomic potentials in cascade simulations in tungsten, J. Nucl. Mater. 470 (2016) 119–127.
[31] K. Nordlund, N. Runeberg, D. Sundholm, Repulsive interatomic potentials calculated using Hartree-Fock and density-functional theory methods, Nucl. Instrum. Methods Phys. Res. B 132 (1) (1997) 45–54.
[32] A. Lopez-Cazalilla, A. Ilinov, F. Djurabekova, K. Nordlund, Modeling of high-fluence irradiation of amorphous Si and crystalline Al by linearly focused Ar ions, J. Phys. Condens. Matter 31 (2018) 075302.
[33] A. Lopez-Cazalilla, F. Djurabekova, A. Ilinov, C. Fridlund, K. Nordlund, Direct observation of ion-induced self-organization and ripple propagation processes in atomistic simulations, Mater. Res. Lett. 8 (3) (2020) 110–116.
[34] D.A. Crowson, D. Farkas, S.G. Corcora, Geometric relaxation of nanoporous metals: The role of surface relaxation, Scr. Mater. 56 (2007) 919–922.
[35] D.A. Crowson, D. Farkas, S.G. Corcora, Mechanical stability of nanoporous metals with small ligament sizes, Scr. Mater. 61 (2009) 497–499.
[36] C. Anders, E.M. Bringa, H.M. Urbassek, Sputtering of a metal nanofoam by Au ions, Nucl. Instrum. Methods Phys. Res. B 342 (2015) 234–239.
[37] A. Stukowski, Visualization and analysis of atomistic simulation data with OVITO – The open visualization tool, Modell. Simul. Mater. Sci. Eng. 18 (2010) 015012.
[38] L. Bukonte, F. Djurabekova, J. Samela, K. Nordlund, S.A. Norris, M.J. Aziz, Comparison of molecular dynamics and binary collision approximation simulations for atom displacement analysis, Nucl. Instrum. Methods Phys. Res. B 297 (2013) 23–28.